

https://doi.org/10.57599/gisoj.2025.5.2.185

Fon A. Zoum¹, Bechan L. Ndimungiang², Menge L. Assamba³

LAND USE/LAND COVER DYNAMICS IN THE GAROUA-BOULAI ARTISANAL GOLD MINING DISTRICT, EAST REGION CAMEROON (2015–2024) USING SENTINEL-2 IMAGERY: A REMOTE SENSING & GIS APPROACH

Abstract: This study examined land use/land cover (LULC) dynamics in the Garoua-Boulai artisanal gold mining district, Cameroon, from 2015 to 2024 using Sentinel-2 imagery, GIS, and statistical analysis. Supervised classification (Maximum Likelihood, ArcGIS 10.8) and accuracy assessment (overall accuracy 87–94%; Kappa 0.80–0.87) revealed major land transformations. Dense vegetation declined by ~48% and agricultural land by ~19%, while bare land expanded by 183%, built-up areas nearly tripled, and mine sites increased by 34%. Correlation analysis showed strong negative relationships between mine sites and vegetation (r = -0.957) and agriculture (r = -0.957) 0.932), and positive relationships with bare land (r = +0.928) and built-up areas (r =+0.997). Regression slopes indicated that each hectare of mine expansion corresponded to losses of \sim 12–17 ha of vegetation/agriculture and gains of \sim 24ha of bare land. Although limited to three temporal data points, the high correlations and explanatory power (R²) provide compelling evidence of mining-driven land change. These findings highlight the urgent need for stronger regulation of artisanal mining, rehabilitation of abandoned pits, and integration of remote sensing into land governance to support sustainable land management in Cameroon's mining districts.

Keywords: ASGM, LULC Change, Sentinel-2 imagery, Remote sensing and GIS, Change detection

Received: 29 August 2025; accepted: 27 October 2025

© 2025 Authors. This is an open access publication, which can be used, distributed and reproduced in any medium according to the Creative Commons CC-BY 4.0 License.

¹ The University of Bamenda, National Higher polytechnic Institute, Department of Mining and Mineral Engineering, Bamenda, Cameroon, ORCID ID: http://orcid.org/0009-0006-4345-3191, email: alainfon4@gmail.com

² The University of Bamenda, National Higher polytechnic Institute, Department of Mining and Mineral Engineering, Bamenda, Cameroon, ORCID ID: http://orcid.org/0009-0001-1943-6782, email: bechanndimungiang@gmail.com

³ The University of Bamenda, National Higher polytechnic Institute, Department of Mining and Mineral Engineering, Bamenda, Cameroon, ORCID ID: http://orcid.org/0009-0008-3585-2621, email: leslieassamba8@gmail.com

Introduction

Natural resources play a vital role in human survival, with land serving as the foundation for terrestrial ecosystem services (Fang et al., 2022). However, mineral resource exploitation, particularly artisanal and small-scale gold mining (ASGM), has become one of the leading drivers of environmental degradation (Ahmad & Pandey, 2018). Mining activities such as excavation, trenching, and sediment reworking often result in deforestation, soil instability, contamination of water bodies, and landscape modifications (Sahu & Er, 2011; Mbaya, 2013; Marangoz et al., 2017). The removal of overburden exposes arable land to erosion, while abandoned pits and unrehabilitated mine sites exacerbate land degradation (Kamga et al., 2020). In addition, ASGM frequently leads to flooding, sedimentation, and biodiversity loss (Gadal et al., 2021), undermining both ecological and economic functions and threatening agricultural sustainability (Basir et al., 2011).

Accurate information on the extent of land degradation caused by mining is essential for policy development and environmental conservation. However, field-based data collection for large areas is often limited, costly, and time-consuming (De Jong, 2015). Remote sensing techniques have therefore emerged as a powerful alternative, offering rapid, cost-effective, and spatially comprehensive monitoring capabilities. In particular, Sentinel-2 satellites under the Copernicus program provide medium-resolution multispectral imagery that is well suited for monitoring short and long-term environmental impacts of mining (Charou et al., 2010).

Globally, several studies have demonstrated the utility of remote sensing in mapping the impacts of gold mining. For example, Caballero-Espejo et al. (2018) used Landsat imagery in the Peruvian Amazon to quantify deforestation linked to ASGM, reporting a dramatic rise in forest loss from 292 ha/year between 2003–2006 to 1,915 ha/year between 2006–2009. In Senegal, Ngom et al. (2020) applied Sentinel-2 and Google Earth Engine to detect ASGM sites, while Lameck et al. (2025) integrated remote sensing with social surveys in Tanzania's Singida Region to assess land use/cover changes and their socio-economic implications. These examples highlight how remote sensing contributes to both environmental monitoring and sustainable land management strategies.

In Cameroon, artisanal gold mining has also been associated with significant environmental degradation across several regions. In the Centre Region, Lum-Ndob et al. (2024) documented a sharp decline in forest cover in the Eseka mining district from 98% in 1990 to 34% in 2022, alongside increases in agricultural land and mining camps. Similarly, Manga et al. (2018) reported extensive deforestation and bare land expansion due to mining activities in the same region. In the Adamawa Region, Tchoua et al. (2024) used Sentinel-2 imagery and photogrammetric analysis to show vegetation and soil deterioration around Mbale, while in the North, Fuh et al. (2023) combined Landsat 8 OLI and Digital Elevation Model (DEM) data to monitor land cover changes associated with mining in the Borongo-Mborguene gold field. Similarly, Mefomdjo et al. (2024)

demonstrated large-scale vegetation loss, soil degradation, and water contamination linked to artisanal mining across northern and eastern gold mining regions.

The East Region, particularly is one of the most affected artisanal gold mining zones. Kamga et al. (2020) reported extensive adverse effects of ASGM on agriculture, health, and education across Betaré-Oya, Ngoura, and Batouri between 1987 and 2017. More recently, Tamfuh et al. (2024) used Sentinel-2 imagery to track land cover changes in Bétaré-Oya between 2018 and 2022, finding rapid mining expansion at the expense of vegetation cover, though a temporary decline occurred during the COVID-19 pandemic.

Despite this growing body of research, limited attention has been given to Garoua-Boulai, another artisanal gold mining district in the East Region. Unlike well-studied areas such as Betaré-Oya, Batouri, and Ngoura, the long-term land use and land cover dynamics in Garoua-Boulai remain poorly understood. Yet, this district is experiencing increasing artisanal mining activity, population influx, and settlement expansion, all of which intensify land degradation pressures. Traditional field surveys for monitoring these changes are often difficult due to terrain, cost, and time constraints (Ahmad & Pandey, 2018), underscoring the need for a rapid and accurate remote sensing-based approach.

This study therefore aims to assess land use and land cover (LULC) dynamics in the Garoua-Boulai artisanal gold mining district between 2015 and 2024 using Sentinel-2 imagery. The specific objectives are to: (i) produce spatial maps of LULC patterns and mining expansion, (ii) quantify transitional changes in LULC for the study period associated with mining, and (iii) establish the relationship between mining activities and land degradation in the district. The findings are expected to advance understanding of ASGM impacts on land systems, contributing baseline knowledge that supports sustainable development.

Material and methods

Description of study area.

Garoua-Boulai is located in the East Region of Cameroon in the Lom and Djerem Division, covering about 2,214 km² (CityPopulation, 2025) and located between 5°25′0″N to 6°0′0″N and14°0′0″ to 15°0′0″E (Fig. 1). Its location on the Douala–Bangui transnational corridor makes it a strategic gateway for trade and migration across the sub region (Humanitarian Data Exchange, 2025). Garoua-Boulai lies on the northeastern margin of the Congo Basin, within a gently dissected plateau transitioning toward the Adamawa highlands. The area belongs to the Lom-Kadey River system, with tributaries originating on the eastern Adamawa Plateau and draining southward into gold-bearing basins. These rivers sustain riparian gallery forests but are increasingly disturbed by artisanal mining (Miles et al., 2006; BRGM, 2024).

The district has a tropical savanna climate characterized by a rainy season from April to November and a dry season from December to March. Mean annual rainfall is \sim 1,500-2,000 mm, with average temperatures of 24-25 °C (Climate-Data.org, 2025). The relatively high elevation (\sim 1,030 m) results in cooler nights. Ecologically, Garoua-Boulaï

belongs to the Northern Congolian forest-savanna mosaic ecoregion, dominated by wooded savannas, semi-deciduous forest patches, and perennial grasses interspersed with agricultural mosaics (WWF, 2025). The natural vegetation is progressively fragmented by logging, smallholder farming, and artisanal gold mining.

The district lies within the Pan-African Central African Fold Belt, specifically the Lom Series, and a Neoproterozoic volcano-sedimentary domain intruded by granitoids and transected by gold-bearing shear zones (Vicat & Pouclet, 1995; Toteu et al., 2001). Weathering of auriferous quartz veins supplies eluvial and alluvial gold to the Lom-Kadey drainage network, which underpins widespread artisanal and semi-mechanized gold mining (ASGM) in the East Region, including Garoua-Boulai, Betare-Oya, Ngoura, and Batouri (BRGM, 2024).

Garoua-Boulai had about 41,000 inhabitants in 2005 (BUCREP, 2010), but recent growth has been driven by cross-border trade and refugee inflows from the Central African Republic (CAR). The nearby Gado-Badzere camp alone has hosted more than 27,000 refugees in recent years (UNHCR, 2023). Population growth, settlement expansion, farming, logging, and ASGM have accelerated land-cover conversion, intensifying environmental pressures.

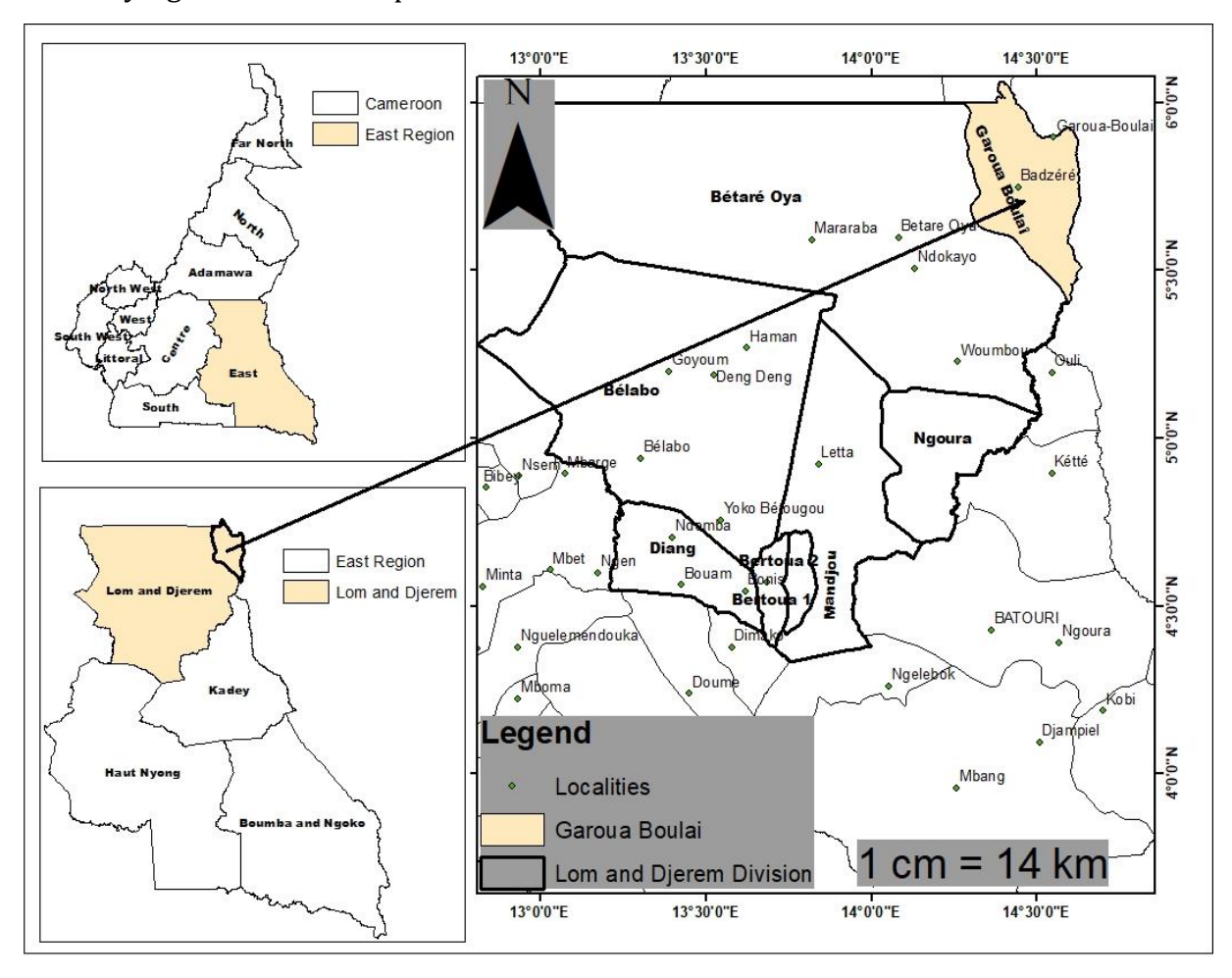


Fig. 1. Location map of study area

Source: Own elaboration

The outline of materials and methods used for land use/land cover (LULC) dynamics monitoring/mapping using Remote Sensing and GIS techniques are described in the flowchart in Fig. 2.

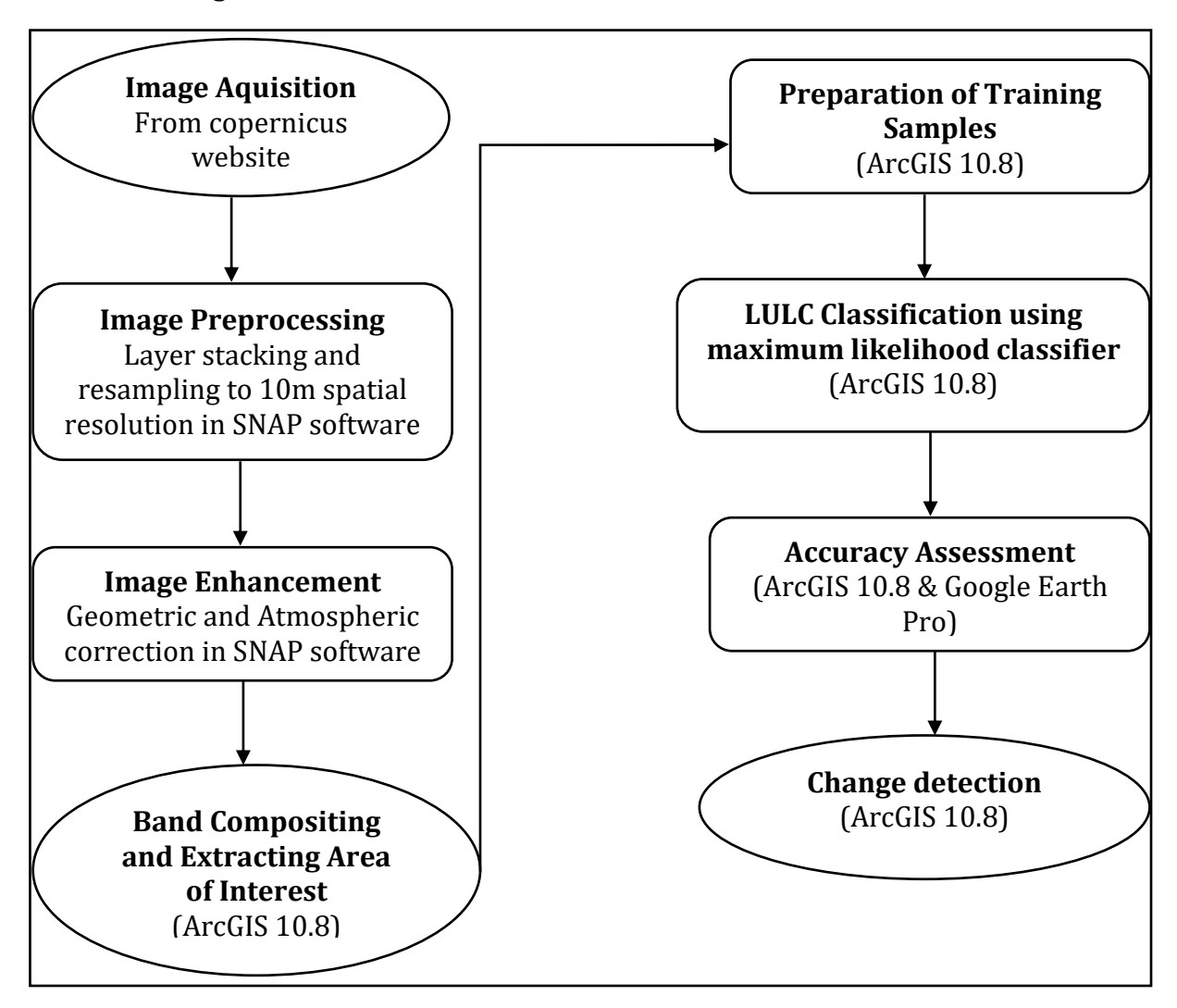


Fig. 2. Flow chart for LULC classification and change detection workflow

Source: Own elaboration

LULC classification, mapping and change dynamics.

Data source and image selection. Sentinel-2 Level-2A images were downloaded from the Copernicus Data Space Ecosystem (https://dataspace.copernicus.eu/). To maximize temporal comparability and reduce seasonal effects, scenes were selected for December of 2015, 2020, and 2024, corresponding to the dry season in the East Region of Cameroon when cloud cover is typically lower and vegetation phenology is relatively stable as shown on Table 1. Sentinel-2 provides 13 spectral bands as seen on Table 2, spanning the visible, near-infrared (NIR), and shortwave infrared (SWIR) regions at native spatial resolutions of 10 m (B2, B3, B4, B8), 20 m (B5, B6, B7, B8A, B11, B12), and 60 m (B1, B9, B10). For each year, all available December scenes with minimal cloud contamination over the area of interest (AOI) were screened using the metadata cloud percentage and quick-look previews; scenes with evident cloud/shadow over the AOI

were excluded. When multiple acceptable scenes were available within the month, they were retained to enable masking and compositing steps that further suppress residual cloud/shadow effects.

Table 1. Characteristics of Sentinel-2 images used for analysis

Year	Satellite	Date of image	Time	Phonological cycle
2015	Sentinel-2 Level 2A	16/12/2015	09:24:12	Dry Season
2020	Sentinel-2 Level 2A	24/12/2020	09:23:19	Dry Season
2024	Sentinel-2 Level 2A	18/12/2024	09:24:11	Dry Season

Source: Own elaboration

Table 2. Sentinel 2 bands characteristics

Sentinel 2 bands	Characteristics	Central wavelength (nm)	Bandwidth (nm)	Spatial resolution (m)	
1	Coastal aerosol	442.7	21	60	
2	Blue	492.4	66	10	
3	Green	559.8	36	10	
4	Red	664.6	31	10	
5	Vegetation red edge	740.5	15	20	
6	Vegetation red edge	740.5	15	20	
7	Vegetation red edge	782.8	20	20	
8	NIR	832.8	106	10	
8A	Narrow NIR	864.7	21	20	
9	Water vapour	945.1	20	60	
10	SWIR - Cirrus	1373.5	31	60	
11	SWIR	1613.7	91	20	
12	SWIR	2202.4	175	20	

Source: Copernicus Data Space Ecosystem, 2025

Pre-processing and image enhancement in SNAP. Image pre-processing was performed in the Sentinel Application Platform (SNAP, ESA). Because Level-2A products are already atmospherically corrected to Bottom-of-Atmosphere (BOA) surface reflectance, the workflow focused on quality masking, geometric harmonization, and spatial resampling. First, the Scene Classification Layer (SCL) provided with L2A (classes for cloud, cloud shadow, vegetation, bare soils, water) and the QA60 mask were used to flag clouds (SCL 8–10), shadows (SCL 3), and snow/ice (SCL 11), which were removed from further processing. A small morphological dilation (1-2 pixels) was applied to the cloud and shadow masks to eliminate edge contamination. All images were checked for map projection consistency and reprojected to UTM Zone 33N (WGS-84) where

necessary to ensure exact co-registration across years. Since Sentinel-2 bands are provided at mixed spatial resolutions, all spectral bands required for classification were resampled to 10m using bilinear interpolation (appropriate for continuous reflectance data) to create a uniform multi-band stack per year. Prior to export, contrast stretching and light histogram normalization were applied to enhance visual interpretability for training-sample delineation.

Band compositing and AOI Extraction. The pre-processed multi-band stacks were imported into ArcGIS Desktop 10.8 (ArcMap). A natural-color composite (Bands 4-3-2) was used for on-screen interpretation and training-sample placement. The AOI was extracted using the clip tool from the toolbox in ArcMap.

Class scheme and training data in ArcGIS Desktop 10.8. Six land-use/land-cover classes were mapped based on local knowledge and visual interpretation: Dense vegetation, Agricultural land, Built-up areas, Water bodies, Bare land, and Mining sites (active pits, tailings, camps, and associated disturbed ground). To capture within-class spectral variability, 150 training samples per class were digitized as polygons distributed across the AOI, avoiding transitional edges and known mixed pixels according to Sathya & Baby (2019).

Supervised classification and post-processing. Supervised classification was carried out using the Maximum Likelihood Classifier (MLC) in ArcGIS, which assigns pixels to the class with the highest posterior probability under the assumption of multivariate normality of class signatures. The signature file generated from the curated training set was used as the classifier input. Class boundaries were visually inspected against the natural-color composite and high-resolution base map tiles; minor manual edits were performed where obvious mislabels occurred.

Area and percentage calculations in ArcGIS 10.8. Area calculations for each year were possible from the final classified raster's summarized attribute tables. Given the 10 m output resolution, each pixel represents 100 m^2 , equivalent to 0.01 ha. Class area (ha) was computed as:

Area (ha) = Pixel Count
$$\times$$
 0.01 (1)

And percentage cover was calculated by dividing class area by the total mapped area and multiplying by 100.

Percentage Cover =
$$\frac{\text{Class Area}}{\text{Total mapped area}} \times 100$$
 (2)

For transparency and reproducibility, all area statistics were generated using the same AOI mask for 2015, 2020, and 2024 to ensure identical denominators across years.

Accuracy assessment. Classification reliability was evaluated using a stratified random sampling design. Independent reference points were generated per class (50 points per class), yielding a validation set that was not used for training (Rwanga & Ndambuki, 2017). Each reference point was interpreted against time-coincident high-resolution imagery in Google Earth Pro (December windows ±1-2 months when necessary). A confusion matrix (error matrix) was then constructed for each year (2015, 2020, and 2024), from which the following standard accuracy metrics were derived:

Producer's Accuracy (PA) and User's Accuracy (UA) for each class, Overall Accuracy (OA), along with the Kappa coefficient to measure agreement beyond chance. The interpretation of Kappa values followed Landis & Koch (1977), Kappa \geq 0.81 was treated as almost perfect agreement, 0.61-0.80 as substantial, 0.41-0.60 as moderate, and values < 0.40 as poor. Accuracy metrics were reported separately for 2015, 2020, and 2024.

Producer's accuracy measures errors of omission, which is a measure of how well real-world land cover types can be classified.

$$Producer's \ Accuracy = \frac{\text{Number of Correctly Cassified Pixels in each Category}}{\text{Total Number of Reference Pixels in that Category}} \times 100$$
 (3)

User's accuracy measures errors of commission, which represents the likelihood of a classified pixel matching the land cover type of its corresponding real-world location.

$$User's \ Accuracy = \frac{\text{Number of Correctly Classified Pixels in each Category}}{\text{Number of Correctly classified Pixels in that Category}} \times 100$$
 (4)

Overall Accuracy is the proportion of correctly classified pixels across all classes relative to the total number of validation samples.

$$Overall\ Accuracy = \frac{\text{Total Correctly classified Samples}}{\text{Total Reference Sample}} \times 100 \tag{5}$$

Change detection. Post-classification comparison was used to detect land cover transitions between 2015-2020, 2020-2024, and 2015-2024. The cross-tabulation method allowed quantification of class-to-class conversions (e.g. dense vegetation to bare land, bare land to mining site, dense vegetation to mining site etc.). This approach minimizes radiometric inconsistencies by relying on classified maps rather than direct image differencing. Transition matrices were generated to capture absolute area changes (ha) between land-cover classes for the periods.

Correlation and regression.

To evaluate the statistical relationships between land-use/land-cover (LULC) classes over time, a correlation and regression analysis was carried out using Microsoft Excel 2013. The analysis was based on the area coverage (ha) of each LULC class (Dense Vegetation, Agricultural Land, Built-up Areas, Water Bodies, Bare Land, and Mine Sites) for the classification years 2015, 2020, and 2024.

Correlation. The Pearson Product-Moment Correlation Coefficient (r) was computed to assess the strength and direction of linear associations between pairs of LULC classes. This coefficient ranges from -1 (perfect negative correlation) to +1 (perfect positive correlation), with values close to 0 indicating weak or no linear relationship. The formula applied in Excel was:

$$r = \frac{\sum (Xi - X)(Yi - Y)}{\sqrt{(\sum (Xi - X)^2 \cdot \sum (Yi - Y)^2)}}$$
 (6)

Where "Xi" and "Yi" represent the observed values of two LULC classes, and "X" and "Y" are their respective means. The resulting correlation matrix allowed identification of inverse relationships (e.g., expansion of mining sites versus decline of dense

vegetation/agriculture) and direct relationships (e.g., growth of bare land alongside mining expansion).

Regression. In addition, simple linear regression was performed to model the dependency of selected LULC classes on mining expansion. Specifically, mine site area (independent variable, X) was regressed against dense vegetation, agricultural land, and bare land (dependent variables, Y). The regression equation applied in Excel was:

$$Y = a + bX \tag{7}$$

Where "Y" is the dependent variable (e.g., vegetation area), "X" is the independent variable (mine sites), "a" is the intercept, "b" is the slope (regression coefficient). The coefficient of determination (R²) was used to measure the proportion of variation in the dependent variable explained by mining expansion. This analysis enabled quantification of how strongly mining growth was associated with land degradation trends (loss of vegetation and agriculture) and land conversion (increase in bare land and built-up areas).

Results and discussion

Land use/Land cover classification results.

The classified maps of 2015, 2020, and 2024 revealed substantial changes in land use and land cover (LULC) within the Garoua-Boulai artisanal gold mining district (Fig. 3). The corresponding class areas and percentages are summarized in Table 3.

Table 3. LULC statistics in Garoua-Boulai (2015–2024)

Year	Class	Area (ha)	Percentage (%)		
	Dense vegetation	30085.13	18.98		
	Agricultural Land	106416.1	67.15		
2015	Built-Up Areas	2262.2	1.43		
2015	Water Bodies	207.69	0.13		
	Bare Land	16474.76	10.40		
	Mine Sites	3049.47	1.92		
	Dense vegetation	25034.47	15.80		
	Agricultural Land	97729.91	61.67		
2020	Built-Up Areas	2854.98	1.80		
2020	Water Bodies	260.49	0.16		
	Bare Land	29481.19	18.60		
	Mine Sites	3121.07	1.97		
	Dense Vegetation	15760.35	9.94		
	Agriculture Land	85742.3	54.10		
2024	Built-up Areas	6130.5	3.87		
2024	Water Bodies	125.5	0.08		
	Bare Land	46635.42	29.43		
	Mine Sites	4088.04	2.58		

Source: Own elaboration

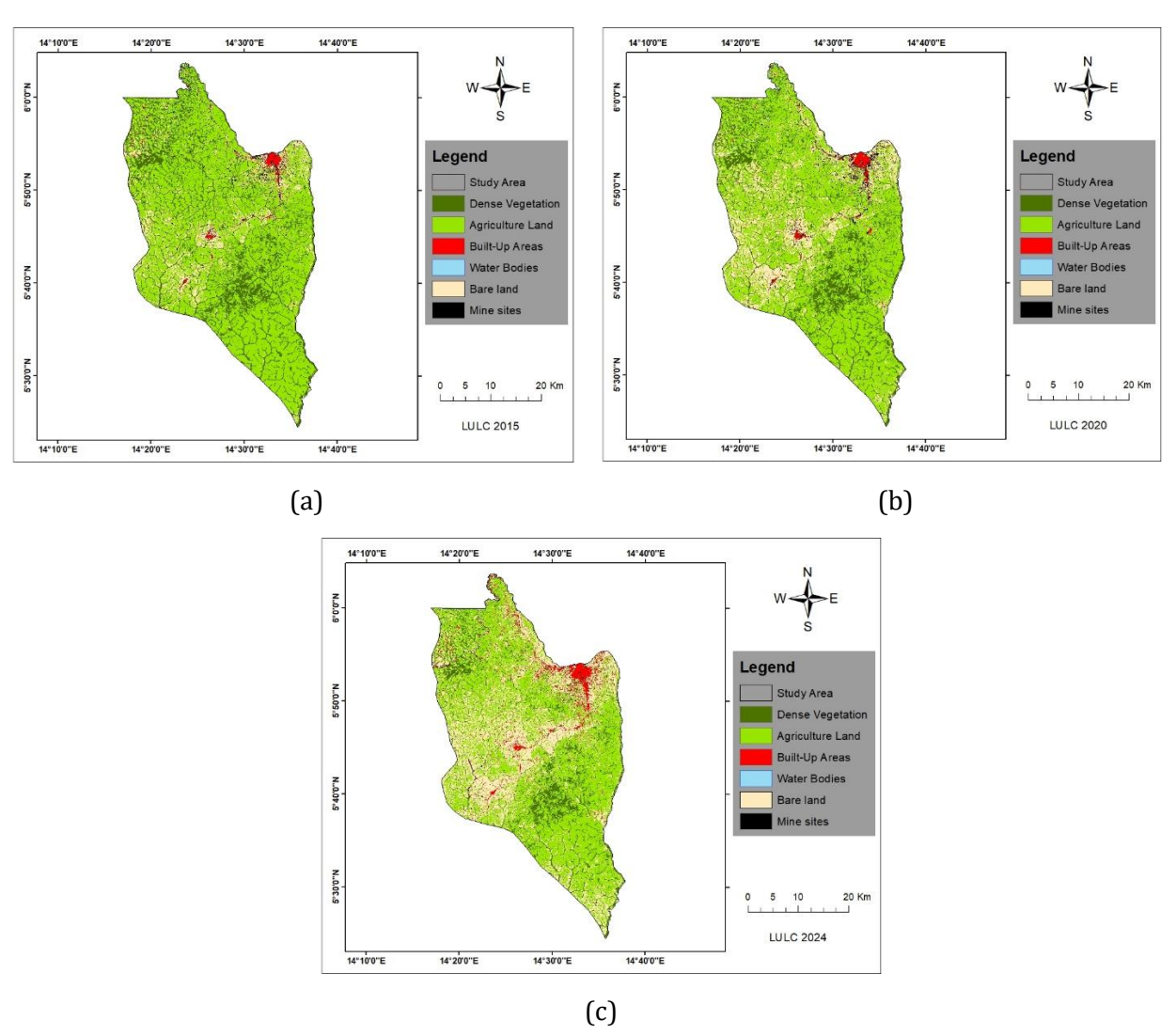


Fig. 3. LULC classified maps for Garoua-Boulai (a) 2015, (b) 2020, (c) 2024

In 2015, agricultural land dominated the landscape (106,416.1 ha; 67.15%), followed by dense vegetation (30,085.1 ha; 18.98%) and bare land (16,474.8 ha; 10.40%). Built-up areas, mining sites, and water bodies were relatively minor, accounting for less than 2% each (see Fig. 3a).

By 2020, agricultural land had declined to 97,729.9 ha (61.67%), and dense vegetation decreased to 25,034.5 ha (15.80%). Meanwhile, bare land increased sharply to 29,481.2 ha (18.60%), while mining sites showed a slight increase to 3,121.1 ha (1.97%), see Fig. 3b.

The 2024 classification shows accelerated land transformation, with agricultural land dropping to 85,742.3 ha (54.10%) and dense vegetation declining further to 15,760.4 ha (9.94%). Bare land expanded dramatically to 46,635.4 ha (29.43%), nearly tripling its 2015 extent. Built-up areas doubled from 2,262.2 ha (2015) to 6,130.5 ha (2024), while mine sites grew to 4,088.0 ha (2.58%). Water bodies remained minimal (<0.2%) throughout the study period (see Fig. 3c).

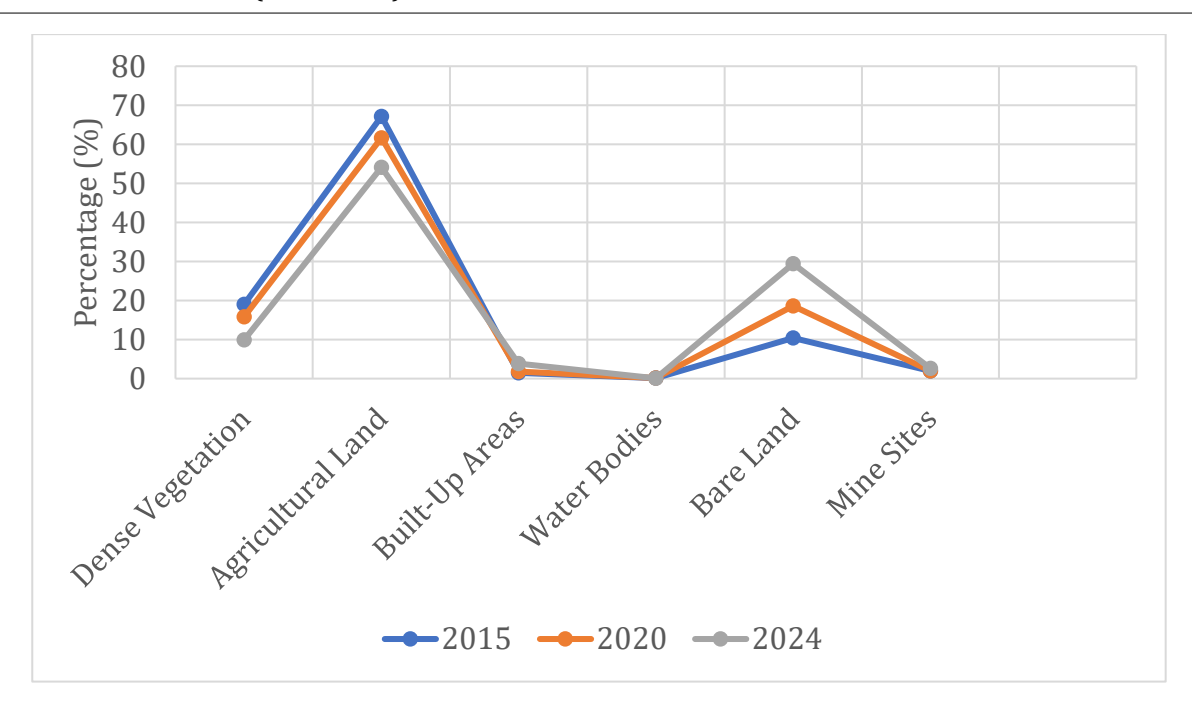


Fig. 4. Trend in LULC in Garoua-Boulai from 2015 to 2024

Figure 4, indicate a clear trajectory of land degradation, marked by the replacement of vegetation and agricultural land with bare land, built-up areas, and mining sites in 2024. The findings align with previous studies in Betare-Oya, East region, Cameron (Kamga et al., 2020; Tamfuh et al., 2024), which reported vegetation loss and agricultural decline due to artisanal mining expansion.

Accuracy assessment results.

The classification reliability was evaluated using independent validation samples and confusion matrices (Table 4). Overall accuracies improved across the three classification years: 87.69% (2015), 89.23% (2020), and 93.85% (2024). The Kappa coefficients were 0.80, 0.81, and 0.87, respectively, indicating substantial to almost perfect agreement according to Landis and Koch (1977).

Producer's and User's accuracies varied by class. For example, mine sites had relatively low User's Accuracy in 2015 (50%) and 2020 (50%), reflecting spectral confusion with bare land and agricultural fields. However, accuracy improved significantly by 2024 (100%). Dense vegetation and agricultural land consistently showed high accuracies, reinforcing the reliability of mapped patterns.

The progressively higher accuracy over time demonstrates the robustness of the classification procedure and validates the subsequent change detection and statistical analyses.

Table 4. Accuracy assessment of LULC classifications (2015–2024)

Class Name	User's Accuracy (%)	Producer's Accuracy (%)			
	2015				
Dense Vegetation	100	54			
Agricultural Land	87	97			
Built-Up Areas	60	100			
Water Bodies	100	67			
Bare Land	100	86			
Mine Sites	50	75			
Overall Accuracy	8'	7.69%			
Kappa Coefficient (K _c)		0.80			
	2020				
Dense Vegetation	95	81			
Agricultural Land	92	95			
Built-Up Areas	50	100			
Water Bodies	100	100			
Bare Land	86	71			
Mine Sites	50	100			
Overall Accuracy	89.23				
Kappa Coefficient (Kc)	0.81				
	2024				
Dense Vegetation	100	86			
Agricultural Land	94	98			
Built-Up Areas	60	100			
Water Bodies	100	100			
Bare Land	95	83			
Mine Sites	100 100				
Overall Accuracy	93.85				
Kappa Coefficient (Kc)	0.87				

Change detection analysis.

Post-classification comparison was used to quantify land-cover transitions (Table 5).

From 2015 to 2020, dense vegetation declined by \sim 5,051 ha, largely converted into agriculture (3,758 ha) and bare land (4,383 ha). Agricultural land decreased by \sim 8,686 ha, with major conversions to bare land (17,268 ha) and mining sites (1,298 ha). Bare land expanded by \sim 13,006 ha, largely at the expense of vegetation and agriculture.

The period between 2020 and 2024, dense vegetation lost \sim 9,274 ha, mainly transitioning into bare land (24,305 ha) and agriculture (7,672 ha). Agricultural land decreased further by \sim 12,000 ha, with significant conversions into bare land (20,511 ha) and mining sites (2,295 ha). Bare land gained \sim 17,154 ha, confirming accelerated degradation. Built-up areas expanded rapidly (+3,276 ha).

For the overall change transition (2015-2024): Dense vegetation declined by \sim 14,325 ha (-47.6%). Agricultural land lost \sim 20,674 ha (-19.4%). Bare land increased by \sim 30,161 ha (+183%). Built-up areas nearly tripled (+3,868 ha). Mine sites expanded by \sim 1,039 ha (+34.1%). These results clearly demonstrate that bare land and mining areas are expanding at the expense of natural vegetation and agriculture, consistent with regional findings in Betare-Oya, Ngoura, and Batouri (Kamga et al., 2020).

Table 5. Transition matrix of LULC Change (2015–2020; 2020–2024; 2015–2024)

Class name		Dense Vegetation	Agricultural Land	Built- Up Areas	Water Bodies	Bare land	Mine Sites	
Dense		2020						
Vegetation		21115.28	8259.61	164.85	29.11	229.18	280.36	
Agricultural Land		3758.41	83200.68	866.4	9.48	17267.68	1297.96	
Built-Up Areas	2015	14.31	508.41	979.3	2.96	469.32	286.35	
Water Bodies		16.58	11.74	3.24	166.34	0.14	8.75	
Bare Land		7.24	4383.3	482.72	0.41	10880.82	714.03	
Mine Sites		117.3	1356.1	358.25	51.98	630.94	533.35	
				2024				
Dense vegetation		14823.58	9620.5	111	0.81	98.08	380.5	
Agricultural Land		919.53	71672.02	2330.5 7	1.91	20511.34	2294.54	
Built-Up Areas	Built-Up 2020		496.1	1489.6 1	0.55	560.54	301.09	
Water Bodies		5.1	22.69	4.7	115.28	0.29	112.43	
Bare Land		0.38	3358.32	1298.7 2	0.42	24305.36	517.99	
Mine Sites		4.67	572.67	895.9	6.53	1159.81	481.49	
		2024						
Dense vegetation		14024.43	14374.71	375.05	2.89	455.23	846.08	
Agricultural Land	S		68478.4	2807.0 1	2.17	31240.54	2174.31	
Built-Up Areas	2015	3.95	286.19	1218.2 2	0.25	608.26	143.78	
Water Bodies		0.9	10.43	6.22	105.49	0.38	83.37	
Bare Land			1596.03	1065.8 5	0.06	13483.17	321.52	
Mine Sites		27.26	987.52	657.69	14.5	842.82	518.13	

These maps as seen in Fig. 5, highlight the spatial distribution, intensity and direction of land cover change, complementing the statistical results presented on Table 5.

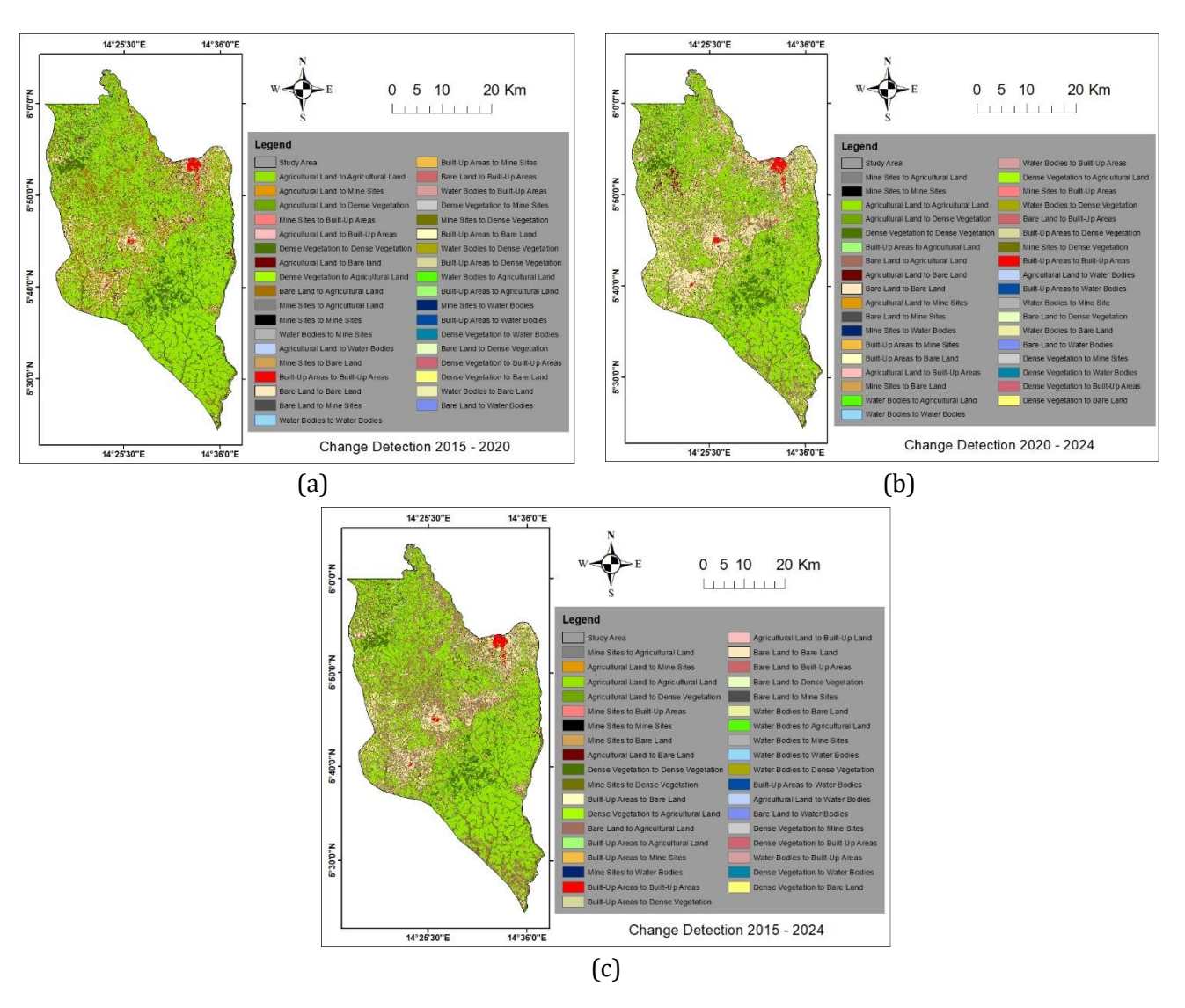


Fig. 5. Change detection maps showing LULC transitions between (a) 2015–2020, (b) 2020–2024, (c) 2015–2024

Correlation and regression analysis.

The statistical analysis provided further evidence of mining-driven land use change in the district.

Correlation results. The Pearson correlation coefficients (Table 6) revealed systematic relationships among LULC classes. Mine sites were strongly and negatively correlated with dense vegetation (r = -0.957) and agricultural land (r = -0.932), confirming that mining expansion occurred largely at the expense of vegetation and agricultural land. In contrast, mine sites exhibited strong positive correlations with bare land (r = +0.928) and built-up areas (r = +0.997), highlighting their role in land degradation and settlement growth.

Table 6. Pearson correlation coefficient (r) between LULC classes (2015–2024)

Variables	Mine Sites	Dense Vegetation	Agricultural Land	Built-Up Areas	Water Bodies	Bare land
Mine Sites	1					
Dense Vegetation	-0.957	1				
Agricultural Land	-0.932	+0.995	1			
Built-Up Areas	+0.997	-0.949	-0.986	1		
Water Bodies	-0.896	+0.965	+0.998	-0.959	1	
Bare land	+0.928	-0.999	-0.986	+0.968	-0.979	1

Water bodies also showed a notable negative correlation with mine sites (r = -0.896), consistent with field observations of riverbank disturbance and ponding in abandoned pits. Agricultural land and dense vegetation were almost perfectly correlated (r = +0.995), indicating their coupled trajectory of decline under mining and settlement pressure.

Regression results. Simple linear regression was used to model the relationships between mine site expansion and other LULC classes (Fig. 6). Dense vegetation vs. mine sites: slope = -11.99; $R^2 = -0.92$; each hectare of mining corresponded to \sim 12ha of vegetation loss (Fig. 6a). Agricultural land vs. mine sites: slope = -16.69; $R^2 = -0.87$; each hectare of mining corresponded to \sim 17ha of farmland loss (Fig. 6b). Bare land vs. mine sites: slope = 24.19; $R^2 = 0.86$; mining expansion coincided with rapid growth of degraded bare land (Fig. 6e). Built-up areas vs. mine sites: slope = 3.58; $R^2 = 0.99$; mining was almost perfectly correlated with settlement expansion, although the scale of land conversion was smaller than for vegetation or agriculture (Fig. 6c). These results confirm that mining is the dominant explanatory factor in land-cover dynamics, simultaneously driving vegetation and agricultural decline while amplifying bare land and settlement growth.

The regression slopes reveal that mining does not merely occupy land directly but also exerts secondary degradation pressures on surrounding landscapes. For example, agricultural plots bordering mine sites are often abandoned due to soil disturbance or waterlogging, while vegetation adjacent to pits is cleared for fuelwood, camps, and informal settlements

Due to limited temporal data points (n = 3), statistical significance was not achieved. However, the very high correlations (|r| > 0.90) and strong explanatory power (R^2) indicates that mining expansion induces land degradation in Garoua-Boulai.

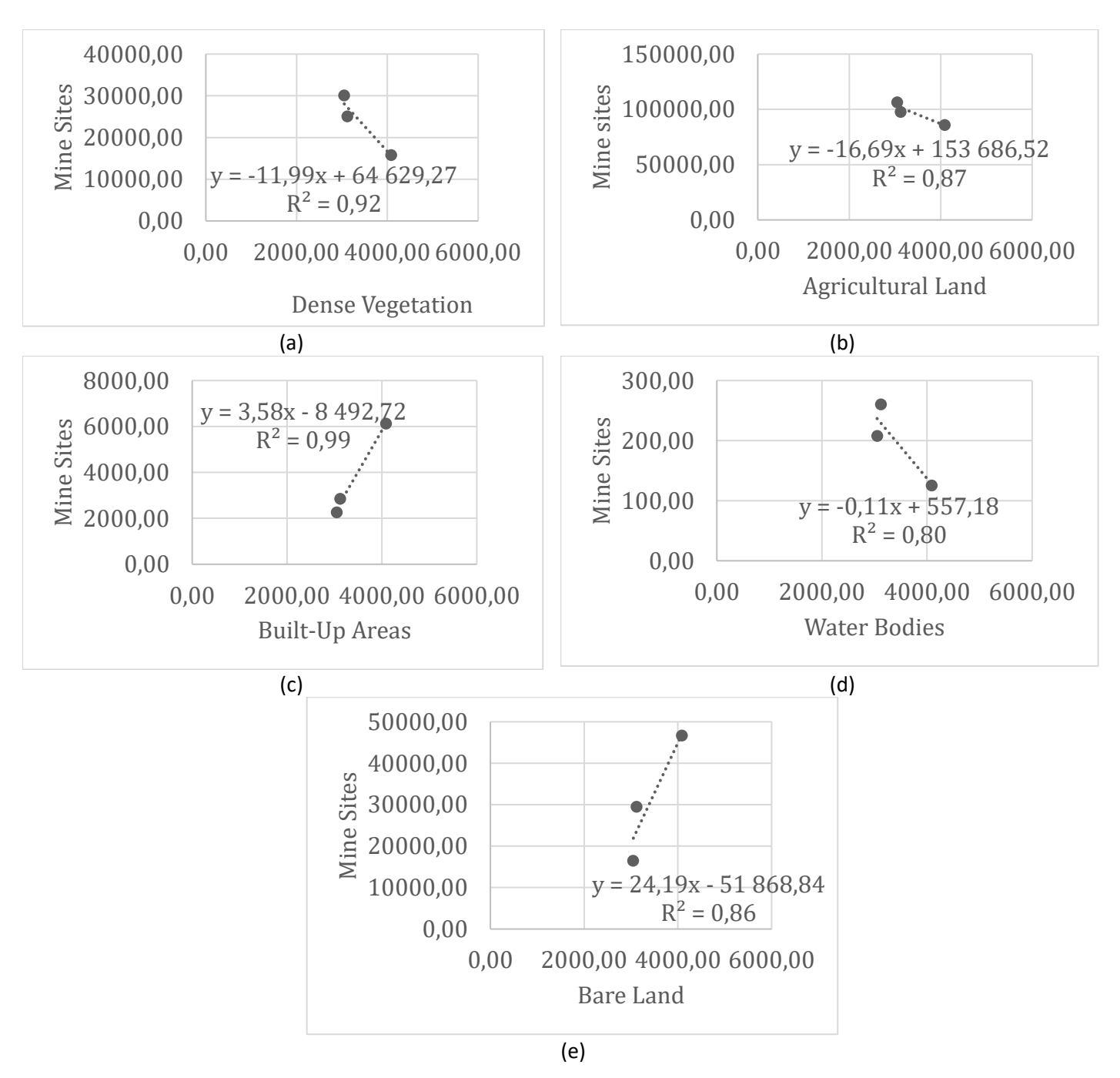


Fig. 6. Regression plots showing the relationships between mine site expansion (independent variable) and (a) dense vegetation, (b) agricultural land, (c) built-Up areas, (d) water bodies, (e) bare land

The observed LULC dynamics in Garoua-Boulai mirror trends reported in other artisanal gold mining regions in sub-Saharan Africa, including Senegal (Ngom et al., 2020), Tanzania (Lameck et al., 2025), and Peru's Amazon (Caballero-Espejo et al., 2018). In all cases, artisanal mining has been linked to accelerated deforestation, soil exposure, and settlement expansion.

In Cameroon, however, research has largely focused on Betare-Oya, Ngoura, and Batouri, leaving Garoua-Boulai understudied. This study demonstrates that Garoua-

Boulai is experiencing equally severe degradation, compounded by population growth, cross-border migration, and refugee inflows from the Central African Republic.

The rapid conversion of vegetation and agricultural land to bare land and mining sites has profound implications for food security, biodiversity conservation, and water resources. Bare land expansion increases vulnerability to erosion and flooding, while agricultural decline undermines local livelihoods. Without intervention, these trends may exacerbate poverty and conflict over natural resources

The observed dynamics can be attributed to multiple interlinked drivers: Expansion of artisanal gold mining pits and semi-mechanized operations, often unregulated; Refugee settlements (Gado-Badzere camp) and migration along the Douala-Bangui corridor intensify land demand; Clearing of vegetation for food production in response to population influx; Growth of built-up areas linked to cross-border trade and mining boomtown effects; Limited enforcement of mining rehabilitation and environmental protection policies. These drivers mirror patterns observed across artisanal mining districts in Africa, where socio-economic pressures compound environmental degradation (Donkor et al., 2006; Ferring & Hausermann, 2019)

Conclusions

This study assessed land use and land cover (LULC) dynamics in the Garoua-Boulai artisanal gold mining district of Cameroon between 2015 and 2024 using Sentinel-2 imagery, supervised classification, accuracy assessment, post-classification change detection, and statistical analysis. The results revealed a progressive and accelerating transformation of the landscape from vegetation and agriculture dominated cover to one increasingly characterized by bare land, mining scars, and expanding settlements.

Between 2015 and 2024, dense vegetation declined by nearly half (-47.6%), agricultural land decreased by \sim 19.4%, while bare land expanded by \sim 183%. Built-up areas nearly tripled, and mine sites grew by \sim 34%. These changes were validated by robust accuracy assessments (overall accuracies of 87–94% and Kappa values of 0.80–0.87), underscoring the reliability of the results. Correlation and regression analyses provided strong statistical evidence that mining expansion is the principal driver of land-cover change. Mining exhibited strong negative correlations with vegetation and agriculture ($r \le -0.93$) and strong positive correlations with bare land and built-up areas ($r \ge +0.92$). Regression slopes indicated that for every hectare of mining expansion, approximately 12–17 ha of vegetation and cropland were lost, while \sim 24 ha of bare land and \sim 3 ha of built-up areas were gained. Although only three temporal data points were available, limiting statistical significance, the strength of correlations (|r| > 0.90) and explanatory power (R^2) provide compelling evidence of mining-driven land use change.

The observed dynamics have profound environmental and socio-economic implications. Vegetation loss reduces biodiversity and carbon sequestration potential, while the decline in cropland threatens food security in a district already pressured by population growth and refugee inflows from the Central African Republic. The expansion of bare land increases vulnerability to erosion, sedimentation, and flooding,

and degraded soils limit prospects for agricultural recovery. Mining activities contribute to landscape fragmentation, water pollution, and health risks from mercury and sediment contamination. At the same time, settlement expansion linked to mining boomtown effects exacerbates land demand and resource conflicts. Collectively, these processes accelerate environmental degradation, undermine sustainable livelihoods, and challenge regional development goals.

In the broader African and global context, the findings align with evidence from other artisanal gold mining regions, including Betare-Oya and Eseka in Cameroon, Senegal, Ghana, Tanzania, and the Peruvian Amazon. This consistency underscores that artisanal mining is a transnational environmental challenge with comparable ecological and social consequences across the tropics.

References

- Ahmad N., Pandey P. (2018). Assessment and Monitoring Of Land Degradation Using Geospatial Technology In Bathinda District, Punjab, India Centre for Environmental Sciences and Technology, Central University of Punjab, Bathinda, Punjab-151001, India. Solid Earth, 9, 75–90.
- Basir C.M., Hasanah U., Nur I., Serikawa Y. (2011). Gold Mining Activities and Its Impacts on Land Degradation in Central Sulawesi Indonesia. Journal of Ecotechnology Research, 16(4):79–83.
- BRGM (2024). Gold Potential of the Lom and Kadey Basins, East Cameroon. Mining and Geology Research Unit, Yaounde.
- BUCREP (2010). Third general population and housing census. Central office for census and population studies, Yaounde.
- Caballero-Espejo J., Messinger M., Roman-Danobeytia F., Ascorra C., Fernandez L.E., Silman M. (2018). Deforestation and forest degradation due to gold mining in the Peruvian Amazon: A 34-year perspective. Remote Sensing, 10(12), 1903. https://doi.org/10.3390/rs10121903.
- Charou E., Stefouli M., Dimitrakopoulos D., Vasiliou E., Mavrantza O. (2010). Using Remote Sensing to Assess Impact of Mining Activities on Land and Water Resources. International Journal of Mine Water, 29(1):45–52.
- CityPopulation (2025). Garoua-Boula (lom and Djerem, Division, Cameroon)-Population Statistics. https://www.citypopulation.de/en/cameroon [access: 20.08.2025].
- Climate-Data.org. (2025). Climate: Garoua-Boulaï, Cameroon. https://en.climate-data.org [access: 20.08.2025].
- Copernicus Data space Ecosystem. https://dataspace.corpenicus.eu/explore-data/data-collections/sentinel-data/sentinel-2 [access: 18.08.2025].
- De Jong M.S., Freek D., Van der M., Jan G.P.W. (2015). Remote Sensing Image Analysis: Including the Spatial Domain. Springer, 1–15.
- Fang Z., Ding T., Chen J., Xue S., Zhou Q., Wang Y., Huang Z., Yang S. (2022). Impacts of Land Use/Land Cover Changes on Ecosystem Services in Ecologically Fragile

- Regions. Science of the Total Environment, 831, article ID: 154967. https://doi.org/10.1016/j.scitotenv.2022.154967.
- Fuh F.T., Tchoua M.T., Tchamba M.N. (2023). Integrating multispectral remote sensing and geological investigations for gold prospecting in the Borongo-Mborguene gold field, Eastern Cameroon. Science of the Total Environment, 850, 157–163.
- Gadal S., Gerard P., Gbetkom A., Mfondoum H.N. (2021). A new soil degradation method analysis by Sentinel-2 images combining spectral indices and statistics analysis: application to the Cameroonian shores of Lake Chad and its hinterland. 7th International Conference on Geographical Information Systems Theory, Applications and Management, pp. 25–36.
- Humanitarian Data Exchange (2025). Cameroon Administrative Boundaries. United Nations OCHA. https://data.humdata.org [accessed 20.08.2025].
- Kamga M.A., Nguemhe F.S.C., Ayodele M.O., Olatubara Ch.O., Nzali S., Adenikinju A., Khalifa M. (2020). Evaluation of land use/land cover changes due to gold mining activities from 1987 to 2017 using Landsat imagery, East Cameroon. GeoJournal, 85, 1097–1114. https://doi.org/10.1007/s10708-019-10067-8.
- Lameck A.S., Rotich B., Czimber K. (2025). Land use and land cover changes due to gold mining in the Singida region, central Tanzania: Environmental and socio-economic implications. Environmental Monitoring and Assessment, 197(4), 1–15. https://doi.org/10.1007/s10661-025-13921-x.
- Lum-Ndob S., Ambo F., Neba A., Ateh I.K., Tata E., Suh C.E. (2024). Land use and land cover dynamics in the Eseka alluvial gold mining district, Centre Region, Cameroon. Journal of Geographic Information System, 16(4), 289–305. https://doi.org/10.4236/jgis.2024.164018.
- Manga E., Kamga A., Nguimfack M. (2018). Spatial Assessment of Impacts of Artisanal and Small-scale Mining on Land Use/Land Cover Changes in the Centre Region of Cameroon. African Journal of Environmental Science and Technology, 12(4), 123–135.
- Marangoz A.M., Sekertekin A., Akçin H. (2017). Analysis of land use land cover classification results derived from sentinel-2 image. Proceedings of the 17th International Multidisciplinary Scientific GeoConference in Surveying Geology and Mining Ecology Management, pp. 25–32.
- Mbaya R.P. (2013). Land Degradation Due To Mining: The Gunda Scenario. International Journal of Geography and Geology, 2(12):144–158.
- Mefomdjo F.B.M., Dairou A.A., Juscar N., Romarice O.M.F., Arsene M., Tchuikoua L.B., Ngueyep L.M. (2024). Assessment of land cover degradation due to mining activities using remote sensing and digital photogrammetry. Environmental Systems Research, 13(1), 41. https://doi.org/10.1186/s40068-024-00372-5.
- Miles L., Newton A.C., DeFries R.S., et al. (2006). A global overview of the conservation status of tropical dry forests. Journal of Biogeography, 33, 491–505.
- Ngom N.M., Mbaye M., Baratoux D., Catry T., Dessay N., Faye G., Sow E.H., Delaitre E. (2020). Mapping artisanal and small-scale gold mining in Senegal using Sentinel 2 Data. GeoHealth, 4, e2020GH000310. https://doi.org/10.1029/2020GH000310.

- Rwanga S., Ndambuki J. (2017). Accuracy Assessment of Land Use/Land Cover Classification Using Remote Sensing and GIS. International Journal of Geosciences, 8, 1–5.
- Sahu H.B., Er S.D. (2011). Land Degradation due to Mining in India and its Mitigation Measures. 2nd International Conference on Environmental Science and Technology, pp. 2–20.
- Sathya P., Baby V. (2019) Classification Process of Satellite Images. International Journal of Computer Application, 9 (1):2250-1797.
- Tamfuh A.P., Ndah, M.E., Nguemhe F.S.C., Ateh K.I., Aye A.B., Tata E., Mamdem L.E., Kenzong B., Kouankap N.G.D., Bitom D. (2024). Mapping land use/land cover changes caused by mining activities from 2018 to 2022 using Sentinel-2 imagery in Betare-Oya (East Cameroon). Journal of Geosciences and Geomatics, 12(1), 12–23. https://doi.org/10.12691/jgg-12-1-3
- Tchoua M.T., Tchamba M.N., Tchoua M.T. (2024). Assessment of land cover degradation due to mining activities using remote sensing in Mbale, Northern Cameroon. Environmental Systems Research, 13(1), 1–15. https://doi.org/10.1186/s40068-024-00372-5
- Toteu S.F., Van Schmus W.R., Penaye J., Nyobé J.B. (2001). U–Pb and Sm–Nd evidence for Eburnean and Pan-African high-grade metamorphism in the Yaounde Group, Cameroon. Precambrian Research, 108, 45–73.
- UNHCR (2023). Cameroon: Gado-Badzéré Refugee Camp Factsheet. United Nations High Commissioner for Refugees.
- Vicat J.P., Pouclet A. (1995). The Neoproterozoic Pan-African belt of Cameroon: A lithostratigraphic, structural and geodynamic review. Journal of African Earth Sciences, 21(3):173–189.
- WWF (2025). Northern Congolian Forest–Savanna Mosaic. World Wildlife Fund Ecoregions Database. https://www.worldwildlife.org/ecoregions/at0723 [access: 20.08.2025].